

# UNITARITY SATURATION IN P-P SCATTERING

Uri Maor

*Raymond and Beverly Sackler Faculty of Exact Science*

*Tel Aviv University, Tel Aviv, 69978, Israel*

**LISHEP March 18-24 2013**

**UERJ Rio de Janeiro, BRASIL**

## INTRODUCTION

This talk aims to assess the approach of p-p scattering toward s and t unitarity saturation. The analysis I shall present is based on:

General principles manifested by Froissart-Martin bound of p-p asymptotic total cross sections, introduced 50 years ago.

TeV-scale p-p data analysis based on the output of the TEVATRON, LHC, and AUGER (in which p-p features are calculated from p-Air Cosmic Rays data).

As we shall see, the TEVATRON(1.8)-LHC(7)-AUGER(57) data indicate that soft scattering amplitudes populate a small, slow growing, fraction of the available phase space confined by unitarity bounds.

Phenomenological unitarity models substantiate the conclusions obtained from the data analysis in the TeV-scale. Model predictions suggest that saturation is attained (if at all) at much higher energies.

A review of updated unitarity models will be given by Gotsman.

## SINGLE CHANNEL UNITARITY

Following are 3 paradoxes, dating back to the ISR epoch, which are resolved by the introduction of unitarity screenings.

- Whereas  $\sigma_{tot}$  grows like  $s^\Delta$ ,  $\sigma_{el}$  grows faster, like  $s^{2\Delta}$  (up to logarithmic corrections). With no screening,  $\sigma_{el}$  will, eventually, be larger than  $\sigma_{tot}$ .
- Elastic and diffractive scatterings are seemingly similar. However, the energy dependence of  $\sigma_{diff}$  is significantly more moderate than that of  $\sigma_{el}$ .
- The elastic amplitude is central in impact parameter b-space, peaking at  $b=0$ . The diffractive amplitudes are peripheral peaking at large b, which gets larger with energy.

Assume a single channel unitarity equation in impact parameter b-space,

$$2\text{Im}a_{el}(s, b) = |a_{el}(s, b)|^2 + G^{inel}(s, b), \quad \text{i.e. at a given (s,b): } \sigma_{el} + \sigma_{inel} = \sigma_{tot}.$$

Its general solution can be written as:

$$a_{el}(s, b) = i \left(1 - e^{-\Omega(s,b)/2}\right) \quad \text{and} \quad G^{inel}(s, b) = 1 - e^{-\Omega(s,b)},$$

where the opacity  $\Omega(s, b)$  is arbitrary. It induces a unitarity bound  $|a_{el}(s, b)| \leq 2$ .

Even though not frequently used, this bound is perfectly legitimate.

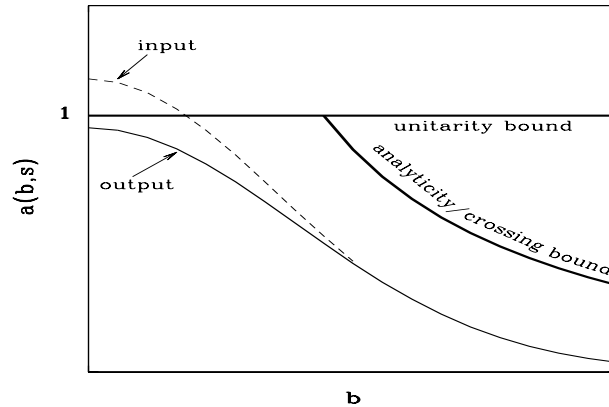
Troshin and Tyurin have promoted a unitarity U matrix model, compatible with the bound above. Their reproduction of the Tevatron data is quite good.

However, their predicted LHC  $\sigma_{el}$  and  $\sigma_{tot}$  values are significantly higher than TOTEM'S 7 TeV cross section data and continue to rapidly grow.

In a Glauber like eikonal approximation, the input opacity,  $\Omega(s, b)$ , is real.

**i.e.  $a_{el}(s, b)$  is imaginary.**  $\Omega$  equals the imaginary part of the input Born term.

The initiated bound is  $|a_{el}(s, b)| \leq 1$ , which is the black disc bound.



In a single channel eikonal model, the screened cross sections are:

$$\sigma_{tot} = 2 \int d^2b \left(1 - e^{-\Omega(s,b)/2}\right), \quad \sigma_{el} = \int d^2b \left(1 - e^{-\Omega(s,b)/2}\right)^2, \quad \sigma_{inel} = \int d^2b \left(1 - e^{-\Omega(s,b)}\right).$$

The figure above shows the effect of s-channel screening, securing that the screened elastic amplitude is bounded by unity. The figure illustrates, also, the bound implied by analyticity/crossing on the expanding b-amplitude.

Saturating s-channel unitarity and analyticity/crossing bounds, we get the

**Froissart-Martin bound:**  $\sigma_{tot} \leq C \ln^2(s/s_0)$ .  $s_0 = 1\text{GeV}^2$ ,  $C = \pi/2m_\pi^2 \simeq 30\text{mb}$ .

C is far too large to be relevant in the analysis of TeV-scale data.

**Coupled to Froissart-Martin is MacDowell-Martin bound:**  $\frac{\sigma_{tot}}{B_{el}} \leq 18 \pi \frac{\sigma_{el}}{\sigma_{tot}}$ .

The Froissart-Martin  $\ln^2 s$  behavior relates to the bound, NOT to the total cross sections which can have any energy dependence as long as  $\sigma_{el}(s)$  is below saturation.

In t-space,  $\sigma_{tot}$  is proportional to a single point,  $d\sigma_{el}/dt(t=0)$  (optical theorem).  $\sigma_{tot}$  in b-space is obtained from a  $b^2$  integration over  $2(1 - e^{-\frac{1}{2}\Omega(s,b)})$ .

Saturation in b-space is, thus, a differential feature, attained initially at  $b=0$  and then expands very slowly with energy.

Consequently, a black core is a product of partial saturation, different from a complete saturation in which  $a_{el}(s,b)$  is saturated at all  $b$ .

In a single channel model,  $\sigma_{el} \leq \frac{1}{2}\sigma_{tot}$  and  $\sigma_{inel} \geq \frac{1}{2}\sigma_{tot}$ .

At saturation, regardless of the energy at which it is attained,  $\sigma_{el} = \sigma_{inel} = \frac{1}{2}\sigma_{tot}$ .

Introducing diffraction, will significantly change the features of unitarity screenings. However, the saturation signatures remain valid.

## TEV-SCALE DATA

Following is p-p TeV-scale data relevant to the assessment of saturation:

**CDF(1.8 TeV):**  $\sigma_{tot} = 80.03 \pm 2.24mb$ ,  $\sigma_{el} = 19.70 \pm 0.85mb$ ,  $B_{el} = 16.98 \pm 0.25GeV^{-2}$ .

**TOTEM(7 TeV):**  $\sigma_{tot} = 98.3 \pm 0.2(stat) \pm 2.8(sys)mb$ ,

$\sigma_{el} = 24.8 \pm 0.2(stat) \pm 1.2(sys)mb$ ,  $B_{el} = 20.1 \pm 0.2(stat) \pm 0.3(sys)GeV^{-2}$ .

**AUGER(57 TeV):**  $\sigma_{tot} = 133 \pm 13(stat) \pm_{20}^{17}(sys) \pm 16(Glauber)mb$ ,

$\sigma_{inel} = 92 \pm 7(stat) \pm_{11}^9(sys) \pm 16(Glauber)mb$ .

**Consequently:**

$\sigma_{inel}/\sigma_{tot}(CDF) = 0.75$ ,  $\sigma_{inel}/\sigma_{tot}(TOTEM) = 0.75$ ,  $\sigma_{inel}/\sigma_{tot}(AUGER) = 0.69$ .

$\sigma_{tot}/B_{el}(TOTEM) = 12.6 < 14.1$ .

The ratios above imply that saturation of the elastic p-p amplitude has NOT been attained up to 57 TeV. Note that the margin of AUGER errors is large. Consequently, present study of saturation in the TeV-scale needs the support of model predictions!

## POMERON MODEL

Translating the concepts presented into a viable phenomenology requires a specification of  $\Omega(s, b)$ , for which Regge poles are a powerful tool.

Pomeron ( $P$ ) exchange is the leading term in the Regge hierarchy.

The growing total and elastic cross sections in the ISR-Tevatron range are well reproduced by the non screened single channel DL  $P$  model in which:

$$\alpha_P(t) = 1 + \Delta_P + \alpha'_P t, \quad \Delta_P = 0.08, \quad \alpha'_P = 0.25 \text{GeV}^{-2}.$$

$\Delta_P$  determines the energy dependence, and  $\alpha'_P$  the forward slopes.

Regardless of DL remarkable success at lower energies, they under estimate the LHC cross sections. This is traced to DL neglect of diffraction and unitarity screenings initiated by s and t dynamics.

Updated Pomeron models include s and t diffraction and unitarity screenings.

## GOOD-WALKER DECOMPOSITION

Consider a system of two orthonormal states, a hadron  $\Psi_h$  and a diffractive state  $\Psi_D$ .  $\Psi_D$  replaces the continuous diffractive Fock states. Good-Walker

(GW) noted that:  $\Psi_h$  and  $\Psi_D$  do not diagonalize the 2x2 interaction matrix  $\mathbf{T}$ .

Let  $\Psi_1, \Psi_2$  be eigen states of  $\mathbf{T}$ .  $\Psi_h = \alpha \Psi_1 + \beta \Psi_2$ ,  $\Psi_D = -\beta \Psi_1 + \alpha \Psi_2$ ,  $\alpha^2 + \beta^2 = 1$ , initiating 4  $A_{i,k}$  elastic GW amplitudes ( $\psi_i + \psi_k \rightarrow \psi_i + \psi_k$ ).  $i,k=1,2$ .

For initial  $p(\vec{p}) - p$  we have  $A_{1,2} = A_{2,1}$ .

I shall follow the GLM definition, in which the mass distribution associated with  $\Psi_D$  is not defined.

The elastic, SD and DD amplitudes in a 2 channel GW model are:

$$a_{el}(s, b) = i\{\alpha^4 A_{1,1} + 2\alpha^2\beta^2 A_{1,2} + \beta^4 A_{2,2}\},$$

$$a_{sd}(s, b) = i\alpha\beta\{-\alpha^2 A_{1,1} + (\alpha^2 - \beta^2)A_{1,2} + \beta^2 A_{2,2}\},$$

$$a_{dd}(s, b) = i\alpha^2\beta^2\{A_{1,1} - 2A_{1,2} + A_{2,2}\}.$$

$$A_{i,k}(s, b) = \left(1 - e^{\frac{1}{2}\Omega_{i,k}(s,b)}\right) \leq 1.$$

GW mechanism changes the structure of s-unitarity below saturation.

- **In the GW sector we obtain the Pumplin bound:**  $\sigma_{el} + \sigma_{diff}^{GW} \leq \frac{1}{2}\sigma_{tot}$ .

$\sigma_{diff}^{GW}$  is the sum of the GW soft diffractive cross sections.

- **Below saturation,**  $\sigma_{el} \leq \frac{1}{2}\sigma_{tot} - \sigma_{diff}^{GW}$  **and**  $\sigma_{inel} \geq \frac{1}{2}\sigma_{tot} + \sigma_{diff}^{GW}$ .

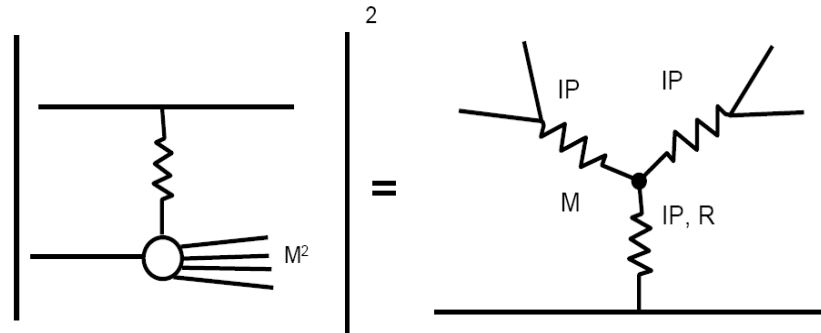
- $a_{el}(s, b) = 1$ , **when and only when,**  $A_{1,1}(s, b) = A_{1,2}(s, b) = A_{2,2}(s, b) = 1$ .

- **When**  $a_{el}(s, b) = 1$ , **all diffractive amplitudes at (s,b) vanish.**

- **As we shall see, there is a distinction between GW and non GW diffraction.**

**Regardless, GW saturation signatures are valid also in the non GW sector.**

- **At saturation,**  $\sigma_{el} = \sigma_{inel} = \frac{1}{2}\sigma_{tot}$ . **In a multi channel calculation we add**  
 $\sigma_{diff} = 0$ . **Consequently, prior to saturation the diffractive cross sections**  
**stop growing and start to decrease with energy!**



## CROSSED CHANNEL UNITARITY

Mueller(1971) applied 3 body unitarity to equate the cross section of

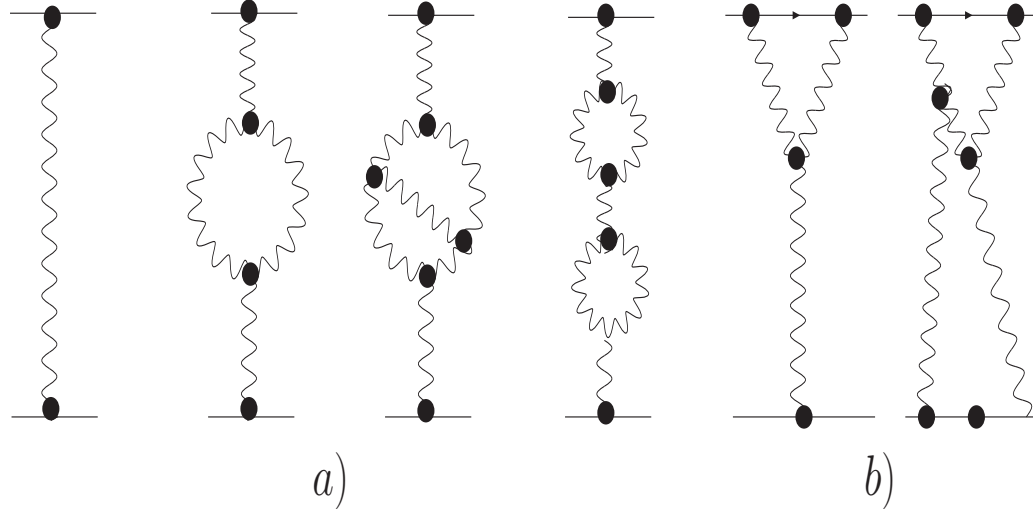
$a + b \rightarrow M_D^2 + b$  to the triple Regge diagram  $a + b + \bar{b} \rightarrow a + b + \bar{b}$ .

The signature of this presentation is a triple vertex with a leading  $3P$  term.

The  $3P$  approximation is valid, when  $\frac{m_p^2}{M_D^2} \ll 1$  and  $\frac{M_D^2}{s} \ll 1$ .

The leading energy/mass dependences are  $\frac{d\sigma^{3P}}{dt dM_D^2} \propto s^{2\Delta_P} \left(\frac{1}{M_D^2}\right)^{1+\Delta_P}$ .

Mueller's  $3P$  approximation for non GW diffraction is the lowest order of multi  $P$  t-channel interactions, which are compatible with t-channel unitarity.



Recall that unitarity screening of GW ("low mass") diffraction is carried out explicitly by eikonalization, while the screening of non GW ("high mass") diffraction is carried out by the survival probability (to be discussed).

The figure above shows the  $IP$  Green function. Multi  $IP$  interactions are summed differently in the various  $IP$  models

Note the analogy with QED renormalization:

- a) Enhanced diagrams, present the renormalization of the propagator.
- b) Semi enhanced diagrams, present the  $pIPp$  vertex renormalization.

## SURVIVAL PROBABILITY

The experimental signature of a  $\mathbb{P}$  exchanged reaction is a large rapidity gap (LRG), devoid of hadrons in the  $\eta - \phi$  lego plot,  $\eta = -\ln(\tan\frac{\theta}{2})$ .

$S^2$ , the LRG survival probability, is a unitarity induced suppression factor of non GW diffraction, soft or hard:  $S^2 = \sigma_{diff}^{scr} / \sigma_{diff}^{nscr}$ . It is the probability that the LRG signature will not be filled by debris (partons and/or hadrons) originating from either the s-channel re-scatterings of the spectator partons, or by the t-channel multi  $\mathbb{P}$  interactions.

Denote the gap survival factor initiated by s-channel eikonalization  $S_{eik}^2$ , and the one initiated by t-channel multi  $\mathbb{P}$  interactions,  $S_{enh}^2$ .

The eikonal re-scatterings of the incoming projectiles are summed over (i,k).

$S^2$  is obtained from a convolution of  $S_{eik}^2$  and  $S_{enh}^2$ .

A simpler, reasonable approximation, is  $S^2 = S_{eik}^2 \cdot S_{enh}^2$ .

## THE PARTONIC POMERON

Current  $\mathbb{P}$  models differ in details, but have in common a relatively large adjusted input  $\Delta_{\mathbb{P}}$  and a very small  $\alpha'_{\mathbb{P}}$ . The exceedingly small fitted  $\alpha'_{\mathbb{P}}$  implies a partonic description of the  $\mathbb{P}$  which leads to a pQCD interpretation. The microscopic sub structure of the  $\mathbb{P}$  is obtained from Gribov's partonic interpretation of Regge theory, in which the slope of the  $\mathbb{P}$  trajectory is related to the mean transverse momentum of the partonic dipoles constructing the Pomeron, and consequently, the running QCD coupling.

$$\alpha'_{\mathbb{P}} \propto 1 / \langle p_t \rangle^2, \quad \alpha_S \propto \pi / \ln \left( \langle p_t^2 \rangle / \Lambda_{QCD}^2 \right) \ll 1.$$

We obtain a single  $\mathbb{P}$  with hardness depending on external conditions.

This is a non trivial relation as the soft  $\mathbb{P}$  is a simple moving pole in J-plane, while, the BFKL  $\mathbb{P}$  is a branch cut approximated, though, as a simple pole with  $\Delta_{\mathbb{P}} = 0.2 - 0.3$ ,  $\alpha'_{\mathbb{P}} = 0$ .

GLM and KMR models are rooted in Gribov's partonic  $\mathbb{P}$  theory with a hard pQCD  $\mathbb{P}$  input. It is softened by unitarity screening (GLM), or the decrease of its partons' transverse momentum (KMR).

Both models have a bound of validity, at 60(GLM) and 100(KMR) TeV, implied by their approximations. Consequently, as attractive as updated  $\mathbb{P}$  models are, we can not utilize them above the TeV-scale.

To this end, the only available models are single channel, most of which have a logarithmic parametrization input. The main deficiency of such models is that while they provide a good reproduction of the total and elastic data at the TeV-scale, their predictions at higher energies are questionable since t-channel screening is not included.

	7 TeV			14 TeV			57 TeV		100 TeV		
	GLM	KMR	BH	GLM	KMR	BH	GLM	BH	GLM	KMR	BH
$\sigma_{tot}$	98.6	97.4	95.4	109.0	107.5	107.3	130.0	134.8	139.0	138.8	147.1
$\sigma_{inel}$	74.0	73.6	69.0	81.1	80.3	76.3	95.2	92.9	101.5	100.7	100.0
$\frac{\sigma_{inel}}{\sigma_{tot}}$	0.75	0.76	0.72	0.74	0.75	0.71	0.73	0.70	0.73	0.73	0.68

## IS SATURATION ATTAINABLE? (PHENOMENOLOGY)

### A) Total and Inelastic Cross Sections:

The Table above, compares  $\sigma_{tot}$  and  $\sigma_{inel}$  outputs of GLM, KMR and BH in the energy range of 7-100 TeV.

Note that, GLM predictions at 100 TeV are above the model validity bound.

As seen, the 3 models have compatible  $\frac{\sigma_{inel}}{\sigma_{tot}}$  outputs in the TeV-scale, significantly larger than 0.5.

The BH model can be applied at arbitrary high energies. The prediction of BH at the Planck-scale ( $1.22 \cdot 10^{16} TeV$ ) is,  $\sigma_{inel}/\sigma_{tot} = 1131mb/2067mb = 0.55$ , which is below  $a_{el}$  saturation.

TeV	1.8 → 7.0	7.0 → 14.0	7.0 → 57.0	57.0 → 100.0	14.0 → 100.0
$\Delta_{eff}(GLM)$	0.081	0.072	0.066	0.060	0.062
$\Delta_{eff}(KMR)$	0.076	0.071			0.065
$\Delta_{eff}(BH)$	0.088	0.085	0.082	0.078	0.080

## B) $\Delta_{\mathcal{P}}^{eff}$ Dependence on Energy:

$\Delta_{\mathcal{P}}^{eff}$  serves as a simple measure of the rate of cross section growth estimated as  $s^{\Delta_{\mathcal{P}}^{eff}}$ . When compared with the adjusted input  $\Delta_{\mathcal{P}}$ , we can assess the strength of the applied screening.

The screenings of  $\sigma_{tot}, \sigma_{el}, \sigma_{sd}, \sigma_{dd}$  and  $M_{diff}^2$  are not identical. Hence, their  $\Delta_{\mathcal{P}}^{eff}$  values are different.

The cleanest determination of  $\Delta_{\mathcal{P}}^{eff}$  is from the energy dependence of  $\sigma_{tot}$ .

All other options require also a determination of  $\alpha'_{\mathcal{P}}$ .

The table above compares  $\Delta_{\mathcal{P}}^{eff}$  values obtained by GLM, KMR and BH.

The continuous reduction of  $\Delta_{\mathcal{P}}^{eff}$  is a consequence of s and t screenings.

	7 TeV		14 TeV		57 TeV	100 TeV	
	GLM	KMR	GLM	KMR	GLM	GLM	KMR
$\sigma_{tot}$	98.6	97.4	109.0	107.5	130.0	134.0	138.8
$\sigma_{el}$	24.6	23.8	27.9	27.2	34.8	37.5	38.1
$\sigma_{sd}^{GW}$	10.7	7.3	11.5	8.1	13.0	13.6	10.4
$\sigma_{sd}$	14.88		17.31		21.68		
$\sigma_{dd}^{GW}$	6.21	0.9	6.79	1.1	7.95	8.39	1.6
$\sigma_{dd}$	7.45		8.38		18.14		
$\frac{\sigma_{el} + \sigma_{diff}^{GW}}{\sigma_{tot}}$	0.42	0.33	0.42	0.34	0.43	0.43	0.36

### C) Diffractive Cross Sections:

GLM and KMR total, elastic and diffractive cross sections are presented.

KMR confine their predictions to the GW sector.

GLM GW  $\sigma_{sd}$  and  $\sigma_{dd}$  are larger than KMR. Their  $\sigma_{tot}$  and  $\sigma_{el}$  are compatible.

In both models, the GW components are compatible with the Pumplin bound.

The persistent growth of the diffractive cross sections indicates that saturation will be attained (if at all) well above the TeV-scale.

Analysis of diffraction, is hindered by different choices of signatures and bounds!

## D) MacDowell-Martin Bound:

Recall that, MacDowell-Martin Bound is  $\frac{\sigma_{tot}}{B_{el}} \leq 18\pi \frac{\sigma_{el}}{\sigma_{tot}}$ .

**GLM and KMR ratios and bounds are:**

$$7\text{TeV} : \frac{\sigma_{tot}}{B_{el}} = 12.5 < 14.1(\text{GLM}), \quad \frac{\sigma_{tot}}{B_{el}} = 12.3 < 13.8(\text{KMR}).$$

$$14\text{TeV} : \frac{\sigma_{tot}}{B_{el}} = 13.0 < 14.5(\text{GLM}), \quad \frac{\sigma_{tot}}{B_{el}} = 12.8 < 14.3(\text{KMR}).$$

$$100\text{TeV} : \frac{\sigma_{tot}}{B_{el}} = 13.8 < 15.3(\text{GLM}), \quad \frac{\sigma_{tot}}{B_{el}} = 13.8 < 15.5(\text{KMR}).$$

**As seen, the ratios above are compatible with a non saturated  $a_{el}(s, b)$  in the TeV-scale.**

## CONCLUSION

**Both the available experimental data in the TeV-scale and the outputs of GLM KMR and BH models, decisively indicate that the p-p elastic amplitude does not saturate up to 100 TeV and possibly (BH) up to the Planck-scale. This conclusion does not rule out the possibility that  $a_{el}(s, b)$  has a black core at high enough energy.**